Research Square

Preprints are preliminary reports that have not undergone peer review.
They should not be considered conclusive, used to inform clinical practice,
or referenced by the media as validated information.

Protecting entanglement properties of Dirac particles in noisy channels in the background of a Schwarzschild black hole

Cookey Iyen

iyen.cookey@fupre.edu.ng

Federal University of Petroleum Resource Effurun

Babatunde James Falaye

Federal University Lafia

Research Article

Keywords: Decoherence, Quantum entanglement, Weak measurement, Black hole, Entanglement protection

Posted Date: October 6th, 2026

DOI: https://doi.org/10.21203/rs.3.rs-11254412/v1

License: This work is licensed under a Creative Commons Attribution 4.0 International License.
Read Full License

Additional Declarations: No competing interests reported.

Protecting entanglement properties of Dirac particles in noisy channels in the background of a Schwarzschild black hole

[1]Cookey Iyen, [2]Babatunde James Falaye

[1] Department of Physics, Federal University of Petroleum Resources, Effurun, Nigeria
[2]Department of Physics, Federal University of Lafia, Nigeria.
[†] Corresponding Author: Cookey Iyen, Department of Physics, Federal University of Petroleum Resources, Effurun, Nigeria, iyen.cookey@fupre.edu.ng

Abstract

Quantum entanglement is a key resource for quantum communication protocols such as quantum cryptography, quantum key distribution (QKD), and quantum secret sharing (QSS), but interactions with the environment can degrade entanglement through decoherence. In this work, weak measurement and post-noise filtration are employed to mitigate entanglement degradation in a tripartite system of entangled Dirac particles interacting with a generalised amplitude damping (GAD) channel and the Hawking radiation associated with a Schwarzschild black hole. Particles A and B are subjected to the GAD channel, whereas particle C is influenced by the Schwarzschild background. The logarithmic negativity is evaluated for the bipartitions $A|BC_1$ and $C_1|AB$. The results show that weak measurement combined with post-noise filtration can enhance the conditional entanglement retained by the system. This enhancement, however, can be accompanied by a reduction in the conditional filtration success probability and the corresponding weighted entanglement yield. Under the parameter regimes considered, the $C_1|AB$ bipartition exhibits a larger relative entanglement enhancement than the $A|BC_1$ bipartition.

keywords: Decoherence, Quantum entanglement, Weak measurement, Black hole, Entanglement protection

1 Introduction

Quantum entanglement is a physical phenomenon in which the quantum states of two or more particles become inseparably correlated, such that measurements performed on one subsystem are correlated with measurements on the others [1, 2, 3, 4]. It is a fundamental resource for quantum communication protocols such as QKD [5, 6, 7] and quantum cryptography [8, 9, 10]. A black hole (BH) is a region of spacetime whose gravitational field is sufficiently strong that nothing crossing the event horizon can escape to infinity, including light [11, 12, 13]. Black holes can be classified according to their charge and angular momentum. Examples include the charged, rotating Kerr–Newman BH [14, 15, 16], the charged, non-rotating Reissner–Nordström BH [17, 18, 19, 20], the rotating, uncharged Kerr BH, and the non-rotating, uncharged Schwarzschild BH [21, 22, 23]. Black-hole spacetimes provide an important setting for studying how relativistic effects influence quantum correlations. In this work, we consider tripartite entangled Dirac particles in the background of a Schwarzschild BH. We focus on an open quantum system whose dynamics are affected by environmental interactions. The generalised amplitude damping channel [24] is used to model dissipative interaction with a finite-temperature environment. Extensive research has examined entanglement evolution in noisy channels [25, 26, 27, 28, 29, 30, 31, 32, 33, 34, 35] and methods for mitigating noise in entanglement-based quantum protocols [36, 37, 38, 39, 40, 41, 42, 43, 26]. For example, Iyen *et al.* [21] investigated quantum Fisher information as a diagnostic tool for entanglement and parameter estimation in a three-qubit entangled Dirac system subjected to a dissipative noisy channel in Schwarzschild spacetime, and reported that squeezing can provide error-mitigation benefits. Sun *et al.* [44] examined entanglement enhancement in an open two-qubit system in a relativistic and noisy setting. To the best of our knowledge, the combined use of weak measurement and post-noise filtration has not been investigated for the present configuration, in which two entangled particles interact with a finite-temperature bath while the third is affected by Hawking radiation from a Schwarzschild BH.

We therefore consider tripartite entangled Dirac particles interacting with a GAD channel and a Schwarzschild BH. The weak-measurement protocol consists of a pre-noise weak measurement followed by a post-noise filtration operation. The weak measurement is applied before the noisy channel, whereas the filtration operation is applied after the noisy interaction.

2 The Kruskal Vacuum near a Schwarzschild BH

The Schwarzschild space-time metric may be expressed as:

$$ds^2 = -(1-\frac{2M}{r})dt^2 + (1-\frac{2M}{r})^{-1}dr^2 + r^2(d\theta^2 + \sin^2\theta\, d\varphi^2), \tag{1}$$

In Eq. (1), M stands for the mass of BH. To simplify the equation, the parameters G, c, $\hbar$, and k_B are assumed to have a value of 1. The Dirac equation that corresponds to the Schwarzschild BH is represented as Eq. (2).

$$[\gamma^a e_a^\mu(\partial_\mu + \Gamma_\mu)]\Psi = 0. \tag{2}$$

By using equations (1) and (2), we derive the Dirac equation for the Schwarzschild space-time, as shown in Eq. (3).

$$-\frac{\gamma_0}{\sqrt{1-\frac{2M}{r}}}\frac{\partial\Psi}{\partial t} + \gamma_1\sqrt{1-\frac{2M}{r}}[\frac{\partial}{\partial r} + \frac{1}{r} + \frac{M}{2r(r-2M)}]\Psi + \frac{\gamma_2}{r}(\frac{\partial}{\partial\theta} + \frac{1}{2}\cot\theta)\Psi + \frac{\gamma_3}{r\sin\theta}\frac{\partial\Psi}{\partial\varphi} = 0. \tag{3}$$

By using the following wavefunction alternative as a parametric substitution:

$$\Psi = (1-\frac{2M}{r})^{-\frac{1}{2}}\begin{pmatrix}\frac{i\zeta_1^{\pm(r)}}{r}\phi_{jm}^{\pm}(\theta,\varphi)\\ \frac{i\zeta_2^{\mp(r)}}{r}\phi_{jm}^{\mp}(\theta,\varphi)\end{pmatrix}e^{-i\omega t}, \tag{4}$$

where the angular harmonics of the spinor are :

$$\phi_{jm}^{+} = \begin{pmatrix}\sqrt{\frac{j+m}{2j}}Y_l^{m-\frac{1}{2}}\\ \sqrt{\frac{j-m}{2j}}Y_l^{m+\frac{1}{2}}\end{pmatrix}, for j = l+\frac{1}{2}, \tag{5}$$

$$\phi_{jm}^{-} = \begin{pmatrix}\sqrt{\frac{j+1-m}{2j+2}}Y_l^{m-\frac{1}{2}}\\ -\sqrt{\frac{j+1+m}{2j+2}}Y_l^{m+\frac{1}{2}}\end{pmatrix}, for j = l-\frac{1}{2}. \tag{6}$$

By solving Eq. (3), we may get the positive frequency outgoing solutions for both the interior and exterior parts of the event horizon as:

$$\begin{aligned}\Psi_k^{II+} &= \mathcal{F}e^{i\omega\mu}, \quad r < r_+,\\ \Psi_k^{I+} &= \mathcal{F}e^{-i\omega\mu}, \quad r > r_+.\end{aligned} \tag{7}$$

The 4-component Dirac spinor $\mathcal{F}$ is defined by:

$$\mathcal{F} = \begin{bmatrix}i(r^4-2Mr^3)^{-\frac{1}{4}}\phi_{jm}^{\pm}(\theta,\varphi)\\ (r^4-2Mr^3)^{-\frac{1}{4}}\phi_{jm}^{\mp}(\theta,\varphi)\end{bmatrix}e^{-i\omega t}, \tag{8}$$

In Eq. (7), the variable μ is defined as the dissimilarity between t and r^*. The value of r^* is obtained by adding r to the product of $2M$ and the natural logarithm of the fraction $\frac{(r-2M)}{(2M)}$, which represents the tortoise coordinates, whereas ω is the monochromatic frequency associated with the Dirac field. The modes are characterised by the wavevector k. The Ψ_k^{II+} and Ψ_k^{I+} constitute a full orthogonal family, which is due to the fact that they are analytic both within and on the exterior of the event horizon. To provide a comprehensive basis for positive modes of energy, we construct an analytical continuation for Eq. (7). The Bogoliubov transformation is obtained by quantising the Dirac field in Schwarzschild and Kruskal spacetimes, as shown in Eq. (9).

$$\begin{bmatrix}c_k^\sigma\\ d_{-k}^{\sigma\dagger}\end{bmatrix} = \mathcal{V}\begin{bmatrix}a_k^\sigma\\ b_{-k}^{\sigma\dagger}\end{bmatrix}\mathcal{V}^{-1}. \tag{9}$$

The variable $\mathcal{V} = exp[r(a_k^{I\dagger} b_{-k}^{II\dagger} + a_k^I b_{-k}^{II})]$ is used to represent a two-mode Dirac squeezing operator. The annihilation and creation operators of the Kruskal vacuum are denoted as c_k and d_k, respectively. The Kruskal vacuum for mode k is obtained by sufficiently normalising the state vector, as shown below:

$$\begin{cases} |0\rangle_K^+ \rightarrow (e^{-\frac{\varpi}{T}} + 1)^{-\frac{1}{2}} |0\rangle_I^+ |0\rangle_{II}^- + (e^{\frac{\varpi}{T}} + 1)^{-\frac{1}{2}} |1\rangle_I^+ |1\rangle_{II}^-, \\ |1\rangle_K^+ \rightarrow |1\rangle_I^+ |0\rangle_{II}^-, \end{cases} \tag{10}$$

where $\{|n_k\rangle_I^+\}$ and $\{|n_k\rangle_{II}^-\}$ denote orthonormal bases for the exterior and interior regions of the event horizon, respectively. $T = (8\pi M)^{-1}$ is the Hawking temperature. The $+$ and $-$ superscripts distinguish particle and antiparticle modes.

3 Materials and Methods

The workflow for the research is as shown in Figure 1.

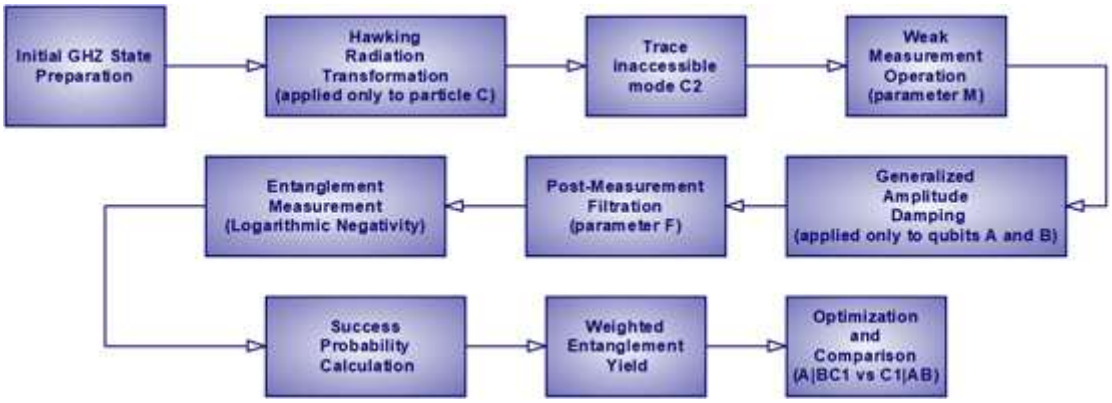


Figure 1: Workflow of the research methodology

The Kraus operators for the GAD channel are given by:

$$\text{Kraus(e_, h_)} := \left\{ \sqrt{p} \begin{pmatrix} 1 & 0 \\ 0 & \sqrt{1-\gamma} \end{pmatrix}, \sqrt{p} \begin{pmatrix} 0 & \sqrt{\gamma} \\ 0 & 0 \end{pmatrix}, \sqrt{1-p} \begin{pmatrix} \sqrt{1-\gamma} & 0 \\ 0 & 1 \end{pmatrix}, \sqrt{1-p} \begin{pmatrix} 0 & 0 \\ \sqrt{\gamma} & 0 \end{pmatrix} \right\}, \tag{11}$$

where γ is the GAD noise parameter and p is the probability of the particle encountering the noise.

The initial measurement operation is given by:

$$M_{wm} = \begin{pmatrix} 1 & 0 \\ 0 & \sqrt{1-M} \end{pmatrix}, \tag{12}$$

The post noise filtration or measurement operation is given by:

$$M_F = \begin{pmatrix} \sqrt{1-F} & 0 \\ 0 & \sqrt{F} \end{pmatrix} \tag{13}$$

3.1 The Bogoliubov transformation for Charlie's particle in the Schwarzschild background

The Kraus operator for the GAD noisy channel is already presented in equation 11.
The selected starting state is a tripartite entangled state that represents the entanglement between three particles labelled A, B, and C.

$$|\chi\rangle_{ABC} = \cos(\theta) |0\rangle_A |0\rangle_B |0\rangle_C + \sin(\theta) e^{i\phi} |1\rangle_A |1\rangle_B |1\rangle_C . \tag{14}$$

Here, θ is the starting entanglement distribution between the two computational basis states, and ϕ is the relative phase. For ease of expression, let the following substitutions be made to equation 14: $a = \cos(\theta)$ and $b = e^{i\phi} \sin(\theta)$, such that equation (14) can be written as:

$$|\psi\rangle_{ABC} = a|000\rangle + b|111\rangle. \tag{15}$$

The corresponding density matrix is given in Eq. (16).

$$\begin{aligned}\rho_{ABC} =&(a|000\rangle + b|111\rangle)(a^*\langle 000| + b^*\langle 111|)\\ =&|a|^2|000\rangle\langle 000| + |b|^2|111\rangle\langle 111|\\ &+ ab^*|000\rangle\langle 111| + a^*b|111\rangle\langle 000|.\end{aligned} \tag{16}$$

When the third particle (Charlie's particle) approaches the event horizon of a Schwarzschild BH, substituting the transformations for $|0\rangle$ and $|1\rangle$ from Eq. (10) and defining $\alpha = \frac{1}{\sqrt{1+e^{-\omega/T_H}}}$ and $\beta = \frac{1}{\sqrt{1+e^{\omega/T_H}}}$ gives Eq. (17).

$$|\Psi\rangle_{ABC_IC_{II}} = a\alpha|000\rangle_{ABC_I}|0\rangle_{C_{II}} + a\beta|001\rangle_{ABC_I}|1\rangle_{C_{II}} + b|111\rangle_{ABC_I}|0\rangle_{C_{II}}. \tag{17}$$

Tracing over the causally inaccessible interior region C_{II} gives the reduced density matrix accessible to observers in region I:

$$\begin{aligned}\rho_{ABC_I} =&|a|^2\alpha^2|000\rangle\langle 000| + |a|^2\beta^2|001\rangle\langle 001|\\ &+ |b|^2|111\rangle\langle 111|\\ &+ a\alpha b^*|000\rangle\langle 111|\\ &+ a^*\alpha b|111\rangle\langle 000|.\end{aligned} \tag{18}$$

This reduced state can be written in matrix form as Eq. (19).

$$\rho_{ABC_I} = \begin{pmatrix} A & 0 & 0 & 0 & 0 & 0 & 0 & C \\ 0 & B & 0 & 0 & 0 & 0 & 0 & 0 \\ 0 & 0 & 0 & 0 & 0 & 0 & 0 & 0 \\ 0 & 0 & 0 & 0 & 0 & 0 & 0 & 0 \\ 0 & 0 & 0 & 0 & 0 & 0 & 0 & 0 \\ 0 & 0 & 0 & 0 & 0 & 0 & 0 & 0 \\ 0 & 0 & 0 & 0 & 0 & 0 & 0 & 0 \\ C^* & 0 & 0 & 0 & 0 & 0 & 0 & D \end{pmatrix} \tag{19}$$

Here, $A = |a|^2\alpha^2$, $B = |a|^2\beta^2$, $D = |b|^2$, and $C = a\alpha b^*$.

3.2 Performing weak measurements on qubits A and B

In our proposed scheme, Alice and Bob perform weak operations on their qubits, encounter the noisy channel and subsequently perform filtering operations on their qubits. This is achieved by applying equation (12) on qubits A and B in the output equation (19). This gives

$$\rho_{WM} = \frac{1}{P_M}\begin{pmatrix} A & 0 & 0 & 0 & 0 & 0 & 0 & C_M \\ 0 & B & 0 & 0 & 0 & 0 & 0 & 0 \\ 0 & 0 & 0 & 0 & 0 & 0 & 0 & 0 \\ 0 & 0 & 0 & 0 & 0 & 0 & 0 & 0 \\ 0 & 0 & 0 & 0 & 0 & 0 & 0 & 0 \\ 0 & 0 & 0 & 0 & 0 & 0 & 0 & 0 \\ 0 & 0 & 0 & 0 & 0 & 0 & 0 & 0 \\ C_M^* & 0 & 0 & 0 & 0 & 0 & 0 & D_M \end{pmatrix}, \tag{20}$$

where the modified coherence and population terms are

$$C_M = (1-M)C, \tag{21}$$

$$D_M = (1-M)^2D, \tag{22}$$

and P_M is the weak-measurement success probability, with $P_M = A + B + D_M = A + B + (1-M)^2D$.

3.3 Action of the GAD channel on qubits A and B

The action of the GAD channel on qubits A and B is achieved by applying equation (11) on the matrix presented in equation (20). This gives rise to the matrix in equation (23):

$$\rho_{\text{GAD}} = \begin{pmatrix} A_G & 0 & 0 & 0 & 0 & 0 & 0 & C_G \\ 0 & B_G & 0 & 0 & 0 & 0 & 0 & 0 \\ 0 & 0 & E_G & 0 & 0 & 0 & 0 & 0 \\ 0 & 0 & 0 & F_G & 0 & 0 & 0 & 0 \\ 0 & 0 & 0 & 0 & E_G & 0 & 0 & 0 \\ 0 & 0 & 0 & 0 & 0 & F_G & 0 & 0 \\ 0 & 0 & 0 & 0 & 0 & 0 & G_G & 0 \\ C_G^* & 0 & 0 & 0 & 0 & 0 & 0 & D_G \end{pmatrix}. \tag{23}$$

Where,

$$A_G = \frac{A(\gamma(p-1)+1)^2}{P_M}$$

,

$$B_G = \frac{B(\gamma(p-1)+1)^2 + D_M\gamma^2p^2}{P_M}$$

,

$$E_G = -\frac{A\gamma(p-1)(\gamma(p-1)+1)}{P_M}$$

,

$$F_G = -\frac{\gamma(B(p-1)(\gamma(p-1)+1) + D_Mp(\gamma p-1))}{P_M}$$

,

$$G_G = \frac{A\gamma^2(p-1)^2}{P_M}$$

,

$$D_G = \frac{B\gamma^2(p-1)^2 + D_M(\gamma p-1)^2}{P_M}$$

,

$$C_G = \frac{(C_M - C_M\gamma)}{P_M}$$

,

$$C_G^* = -\frac{(\gamma-1)C_M^*}{P_M}$$

3.4 Post noise filtration on the particles A and B

The filtration operation on particles A and B after they encounter a noisy channel is achieved by applying equation 13 on the output gotten from equation 23. We obtain:

$$\widetilde{\rho}_F = \begin{pmatrix} F_1 & 0 & 0 & 0 & 0 & 0 & 0 & F_9 \\ 0 & F_2 & 0 & 0 & 0 & 0 & 0 & 0 \\ 0 & 0 & F_3 & 0 & 0 & 0 & 0 & 0 \\ 0 & 0 & 0 & F_4 & 0 & 0 & 0 & 0 \\ 0 & 0 & 0 & 0 & F_5 & 0 & 0 & 0 \\ 0 & 0 & 0 & 0 & 0 & F_6 & 0 & 0 \\ 0 & 0 & 0 & 0 & 0 & 0 & F_7 & 0 \\ F_9^* & 0 & 0 & 0 & 0 & 0 & 0 & F_8 \end{pmatrix}. \tag{24}$$

$$F_1 = \frac{A(F-1)(F^*-1)\left[\gamma(p-1)+1\right]^2}{\mathrm{PM}},$$

$$F_2 = \frac{(F-1)(F^*-1)\left[B\left[\gamma(p-1)+1\right]^2+\gamma^2\mathrm{DM}\,p^2\right]}{\mathrm{PM}},$$

$$F_3 = -\frac{A\gamma(p-1)\left|(F-1)F\right|\left[\gamma(p-1)+1\right]}{\mathrm{PM}},$$

$$F_4 = -\frac{\gamma\left|(F-1)F\right|\left[B(p-1)\left[\gamma(p-1)+1\right]+\mathrm{DM}\,p(\gamma p-1)\right]}{\mathrm{PM}},$$

$$F_5 = F_3,$$

$$F_6 = F_4,$$

$$F_7 = \frac{A\gamma^2F(p-1)^2F^*}{\mathrm{PM}},$$

$$F_8 = \frac{FF^*\left[B\gamma^2(p-1)^2+\mathrm{DM}(\gamma p-1)^2\right]}{\mathrm{PM}},$$

$$F_9 = \frac{(\gamma-1)\mathrm{CM}(F-1)F^*}{\mathrm{PM}}.$$

$$F_9^* = \frac{(\gamma-1)F\,\mathrm{CM}^*(F^*-1)}{\mathrm{PM}}.$$

The normalized post-filtration state is $\rho_F = \widetilde{\rho}_F/P_F$, where $P_F = \mathrm{Tr}(\widetilde{\rho}_F)$.

3.5 Logarithmic negativity for the bipartition $A|BC_1$

Taking the partial transpose of the normalized filtered density matrix with respect to subsystem A moves the coherence terms from $(1,8)$ and $(8,1)$ to the subspace connecting $|011\rangle$ and $|100\rangle$. The resulting matrix is

$$\rho_F^{T_A} = \frac{1}{P_F}\begin{pmatrix} a_1 & 0 & 0 & 0 & 0 & 0 & 0 & 0 \\ 0 & a_2 & 0 & 0 & 0 & 0 & 0 & 0 \\ 0 & 0 & a_3 & 0 & 0 & 0 & 0 & 0 \\ 0 & 0 & 0 & a_4 & c & 0 & 0 & 0 \\ 0 & 0 & 0 & c^* & a_3 & 0 & 0 & 0 \\ 0 & 0 & 0 & 0 & 0 & a_4 & 0 & 0 \\ 0 & 0 & 0 & 0 & 0 & 0 & a_7 & 0 \\ 0 & 0 & 0 & 0 & 0 & 0 & 0 & a_8 \end{pmatrix} \tag{25}$$

$$
\begin{aligned}
a_1 &= \frac{A(F-1)(F^*-1)(\gamma(p-1)+1)^2}{PM},\\
a_2 &= \frac{(F-1)(F^*-1)\left[B(\gamma(p-1)+1)^2+DM\gamma^2p^2\right]}{PM},\\
a_3 &= -\frac{A\gamma(p-1)|(F-1)F|(\gamma(p-1)+1)}{PM},\\
a_4 &= -\frac{\gamma|(F-1)F|\left[B(p-1)(\gamma(p-1)+1)+DMp(\gamma p-1)\right]}{PM},\\
c &= \frac{F(\gamma-1)CM^*(F^*-1)}{PM},\\
c^* &= \frac{CM(F-1)(\gamma-1)F^*}{PM},\\
a_7 &= \frac{AF\gamma^2(p-1)^2F^*}{PM},\\
a_8 &= \frac{FF^*\left[B\gamma^2(p-1)^2+DM(\gamma p-1)^2\right]}{PM}.
\end{aligned}
\tag{26}
$$

The two eigenvalues associated with the non-trivial 2×2 block

$$
\frac{1}{P_F}\begin{pmatrix} a_4 & c \\ c^* & a_3 \end{pmatrix} \tag{27}
$$

are

$$
\lambda_\pm = \frac{a_3+a_4\pm\Delta}{2P_F}, \tag{28}
$$

where

$$
\Delta = \sqrt{(a_4-a_3)^2+4|c|^2}. \tag{29}
$$

The complete eigenvalue spectrum is therefore

$$
\Lambda(\rho_F^{T_A}) = \left\{\frac{a_1}{P_F},\frac{a_2}{P_F},\frac{a_3}{P_F},\frac{a_4}{P_F},\frac{a_7}{P_F},\frac{a_8}{P_F},\frac{a_3+a_4+\Delta}{2P_F},\frac{a_3+a_4-\Delta}{2P_F}\right\}. \tag{30}
$$

The eigenvectors associated with the six uncoupled eigenvalues are the standard basis vectors,

$$
\begin{aligned}
|v_1\rangle &= (1,0,0,0,0,0,0,0)^T,\\
|v_2\rangle &= (0,1,0,0,0,0,0,0)^T,\\
|v_3\rangle &= (0,0,1,0,0,0,0,0)^T,\\
|v_4\rangle &= (0,0,0,0,0,1,0,0)^T,\\
|v_5\rangle &= (0,0,0,0,0,0,1,0)^T,\\
|v_6\rangle &= (0,0,0,0,0,0,0,1)^T.
\end{aligned}
\tag{31}
$$

For the coupled block, the normalized eigenvectors may be written as

$$
|v_\pm\rangle = \frac{1}{\sqrt{1+|r_\pm|^2}}(0,0,0,1,r_\pm,0,0,0)^T, \tag{32}
$$

with

$$
r_\pm = -\frac{a_4-\lambda_\pm P_F}{c}. \tag{33}
$$

The negativity is

$$
\mathcal{N}_{A|BC_1} = \frac{\max\left[0,\Delta-(a_3+a_4)\right]}{2P_F}, \tag{34}
$$

and the condition for non-zero negativity is

$$
|c|^2 > a_3a_4. \tag{35}
$$

Hence, the logarithmic negativity is

$$E_N^{A|BC_1} = \log_2 \left[1 + \frac{\max\left[0, \sqrt{(a_4 - a_3)^2 + 4|c|^2} - (a_3 + a_4)\right]}{P_F} \right]. \tag{36}$$

3.6 Logarithmic negativity for the bipartition $C_1|AB$

To quantify entanglement across the partition containing the particle directly affected by the Schwarzschild background, the partial transpose is taken with respect to Charlie's accessible subsystem. Following the same procedure used for $A|BC_1$, the physically relevant Hawking partition is

$$C_I|AB. \tag{37}$$

The partial transpose is therefore taken with respect to the third subsystem.
Under T_C,

$$|000\rangle\langle 111| \longrightarrow |001\rangle\langle 110|, \tag{38}$$

and

$$|111\rangle\langle 000| \longrightarrow |110\rangle\langle 001|. \tag{39}$$

Hence,

$$\rho_F^{T_C} = \frac{1}{P_F} \begin{pmatrix} f_0 & 0 & 0 & 0 & 0 & 0 & 0 & 0 \\ 0 & f_1 & 0 & 0 & 0 & 0 & c_F & 0 \\ 0 & 0 & f_2 & 0 & 0 & 0 & 0 & 0 \\ 0 & 0 & 0 & f_3 & 0 & 0 & 0 & 0 \\ 0 & 0 & 0 & 0 & f_4 & 0 & 0 & 0 \\ 0 & 0 & 0 & 0 & 0 & f_5 & 0 & 0 \\ 0 & c_F^* & 0 & 0 & 0 & 0 & f_6 & 0 \\ 0 & 0 & 0 & 0 & 0 & 0 & 0 & f_7 \end{pmatrix}. \tag{40}$$

The non-trivial block is therefore

$$\frac{1}{P_F} \begin{pmatrix} f_1 & c_F \\ c_F^* & f_6 \end{pmatrix}. \tag{41}$$

The eigenvalues of this block satisfy

$$\det \begin{pmatrix} f_1 - \lambda P_F & c_F \\ c_F^* & f_6 - \lambda P_F \end{pmatrix} = 0. \tag{42}$$

Therefore,

$$\lambda_{\pm}^{(C)} = \frac{f_1 + f_6 \pm \sqrt{(f_1 - f_6)^2 + 4|c_F|^2}}{2P_F}. \tag{43}$$

The remaining eigenvalues are

$$\frac{f_0}{P_F}, \quad \frac{f_2}{P_F}, \quad \frac{f_3}{P_F}, \quad \frac{f_4}{P_F}, \quad \frac{f_5}{P_F}, \quad \frac{f_7}{P_F}. \tag{44}$$

The smaller eigenvalue is negative only when

$$|c_F|^2 > f_1 f_6. \tag{45}$$

The negativity for the Hawking partition is therefore

$$\mathcal{N}_{C|AB} = \frac{\max\left[0, \sqrt{(f_1 - f_6)^2 + 4|c_F|^2} - f_1 - f_6\right]}{2P_F}. \tag{46}$$

Hence the corrected logarithmic negativity is

$$E_N^{C|AB} = \log_2 \left[1 + \frac{\max\left[0, \sqrt{(f_1 - f_6)^2 + 4|c_F|^2} - f_1 - f_6\right]}{P_F} \right] \tag{47}$$

with

$$f_1 = (1-F)^2 \frac{B[1+\gamma(p-1)]^2 + D_M \gamma^2 p^2}{P_M}, \tag{48}$$

$$f_6 = F^2 \frac{A\gamma^2(1-p)^2}{P_M}, \tag{49}$$

and

$$c_F = \frac{F(1-F)(1-\gamma)(1-M)C}{P_M}. \tag{50}$$

Using

$$C = \cos(\theta)\sin(\theta)e^{-i\phi}\left(1 + e^{-\omega/T_H}\right)^{-1/2}, \tag{51}$$

the modulus of the coherence is

$$|C| = |\cos(\theta)\sin(\theta)|\left(1 + e^{-\omega/T_H}\right)^{-1/2}. \tag{52}$$

Therefore,

$$|c_F| = \frac{F(1-F)(1-\gamma)(1-M)|\cos(\theta)\sin(\theta)|}{P_M\sqrt{1+e^{-\omega/T_H}}}. \tag{53}$$

The corrected logarithmic negativity consequently depends on

$$E_N^{C_1|AB} = E_N\left(M, F, T_H, \gamma, p, \theta, \omega\right), \tag{54}$$

3.7 Conditional filtration success probability

The quantity P_F used here is the probability that the post-noise filtration succeeds, conditional on a successful weak-measurement outcome. It is determined by the filtration operation and is independent of the bipartition used to evaluate entanglement. The total success probability of the full probabilistic protocol would be $P_{\text{tot}} = P_M P_F$.

Following the generalized amplitude damping transformation, the probabilistic filtration operation is applied to the resulting normalized post-weak-measurement state. The unnormalized filtered density matrix is defined as

$$\widetilde{\rho}_F = \mathcal{F}\rho_{\text{GAD}}\mathcal{F}^\dagger, \tag{55}$$

where the local filtering operator is

$$\mathcal{F} = F_f^{(A)} \otimes F_f^{(B)} \otimes I^{(C)}, \tag{56}$$

with

$$F_f = \begin{pmatrix} \sqrt{1-F} & 0 \\ 0 & \sqrt{F} \end{pmatrix}. \tag{57}$$

The filtered matrix elements are

$$f_0 = (1-F)^2 g_0, \qquad f_1 = (1-F)^2 g_1, \tag{58}$$

$$f_2 = F(1-F)g_2, \qquad f_3 = F(1-F)g_3, \tag{59}$$

$$f_4 = F(1-F)g_4, \qquad f_5 = F(1-F)g_5, \tag{60}$$

$$f_6 = F^2 g_6, \qquad f_7 = F^2 g_7, \tag{61}$$

and the filtered coherence becomes

$$c_F = F(1-F)C_G. \tag{62}$$

The probability that the filtering operation succeeds is obtained from the trace of the unnormalized filtered state:

$$P_F = \mathrm{Tr}(\widetilde{\rho}_F) \tag{63}$$

which gives

$$P_F = f_0 + f_1 + f_2 + f_3 + f_4 + f_5 + f_6 + f_7. \tag{64}$$

Substituting the filtered populations yields

$$P_F = (1-F)^2(g_0+g_1) + F(1-F)(g_2+g_3+g_4+g_5) + F^2(g_6+g_7) \tag{65}$$

Using the symmetry relations

$$g_2 = g_4, \qquad g_3 = g_5, \tag{66}$$

the success probability can be written as

$$P_F = (1-F)^2(g_0+g_1) + 2F(1-F)(g_2+g_3) + F^2(g_6+g_7). \tag{67}$$

The generalized amplitude damping populations are

$$g_0 = \frac{Ar^2}{P_M}, \tag{68}$$

$$g_1 = \frac{Br^2 + D_M t^2}{P_M}, \tag{69}$$

$$g_2 = g_4 = \frac{Ars}{P_M}, \tag{70}$$

$$g_3 = g_5 = \frac{Brs + D_M tu}{P_M}, \tag{71}$$

$$g_6 = \frac{As^2}{P_M}, \tag{72}$$

$$g_7 = \frac{Bs^2 + D_M u^2}{P_M}, \tag{73}$$

where

$$r = 1 - \gamma(1-p), \tag{74}$$

$$s = \gamma(1-p), \tag{75}$$

$$t = \gamma p, \tag{76}$$

$$u = 1 - \gamma p. \tag{77}$$

Therefore, the fully expanded filtration success probability is

$$\begin{aligned} P_F = \frac{1}{P_M}\Big[&(1-F)^2\left((A+B)r^2 + D_M t^2\right) \\ &+ 2F(1-F)\left((A+B)rs + D_M tu\right) \\ &+ F^2\left((A+B)s^2 + D_M u^2\right)\Big]. \end{aligned} \tag{78}$$

Equation (78) gives the conditional filtration success probability P_F. When the probability of the preceding weak-measurement outcome is also included, the full protocol success probability is $P_{\mathrm{tot}} = P_M P_F$.

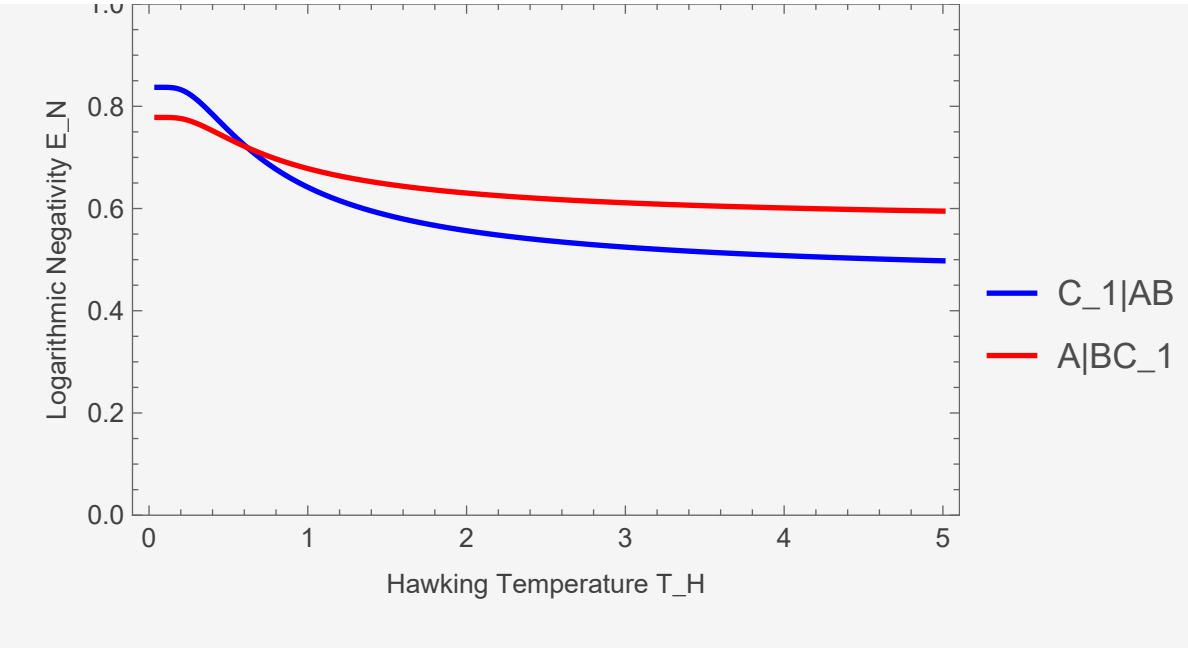


Figure 2: Plot showing Entanglement variation for both bipartitions $A|BC_1$ and $C_1|AB$

3.8 Conditional weighted entanglement yield for C1—AB

Using the conditional filtration success probability defined above, the corresponding conditional weighted entanglement yield is given by Eq. (79).

$$Y_E = P_F E_N^{C_1|AB} \tag{79}$$

or explicitly, by substituting equations (47) and (78) into equation (79), we obtain the equation for the weighted entanglement yield for the $C_1|AB$ bipartition as presented in equation (80).

$$Y_E^{C_1|AB} = P_F \log_2 \left[1 + \frac{1}{P_F} \max \left(0, \sqrt{(f_1 - f_6)^2 + 4|c_F|^2} - f_1 - f_6 \right) \right]. \tag{80}$$

3.9 Conditional weighted entanglement yield for A—BC1

Following the same procedure as in subsection (3.8), the conditional weighted entanglement yield for $A|BC_1$ is given by Eq. (81).

$$Y_E^{A|BC_I} = P_F \log_2 \left[1 + \frac{\max \left(0, \sqrt{[F(1-F)(g_3 - g_4)]^2 + 4|c_F|^2} - F(1-F)(g_3 + g_4) \right)}{P_F} \right] \tag{81}$$

4 Results and Discussions

Weak measurement was performed on Alice's and Bob's qubits before they encountered the GAD channel, while filtration was performed after they encountered the GAD channel. The plots show the characteristics of the entanglement with variations in different associated parameters.

Figure (2) shows the variation of log negativity with rising values of Hawking temperature T_H for bipartitions $A|BC_1$ and $C_1|AB$ for the scenario when the weak measurement (WM) parameter $M = 0$ and the post-noise filtration (PNF) parameter $F = 0.5$, which according to our protocol is equivalent to a filtration of identity. For the bipartition $A|BC_1$, it is observed that the log negativity drops from 0.778

to 0.595 with increasing T_H, which is about a 23.52% decline in log negativity, while for the bipartition $C_1|AB$, it recorded a decline from 0.837 to 0.498, which is about a 40.5% decline in log negativity. This shows that T_H has a more adverse effect on the bipartition $C_1|AB$ relative to C_1 of the qubit that is in the environment of the BH than on the other bipartition $A|BC_1$, and from the plot, it is clear that T_H does not lead to entanglement sudden death in both bipartitions under consideration.

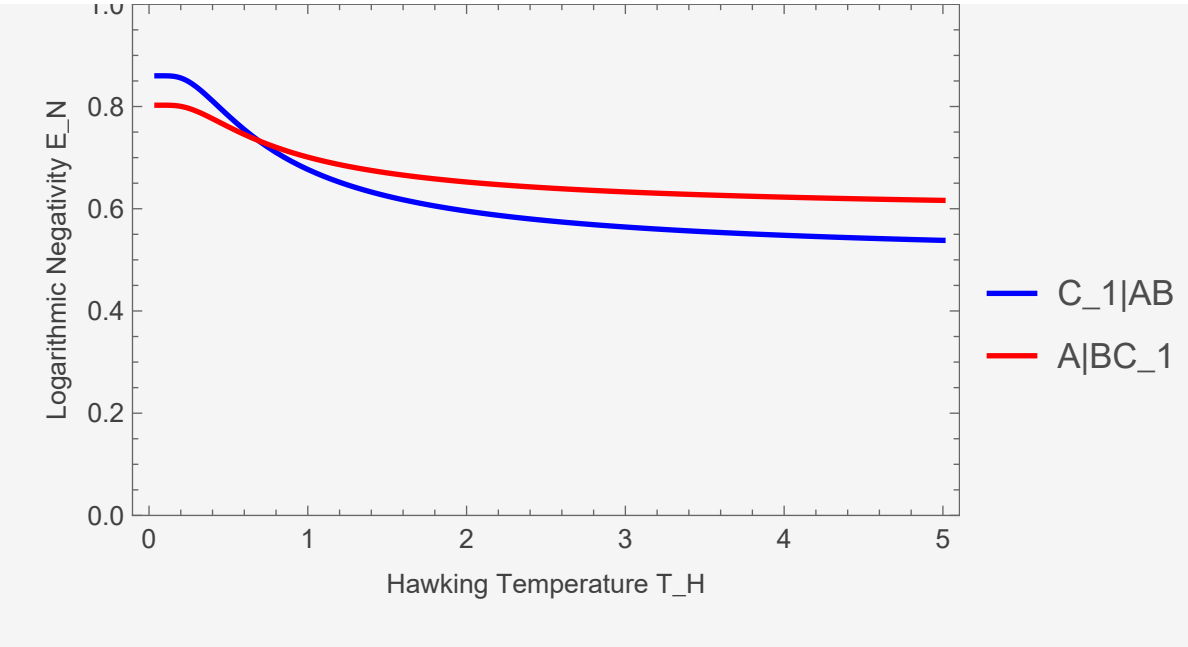


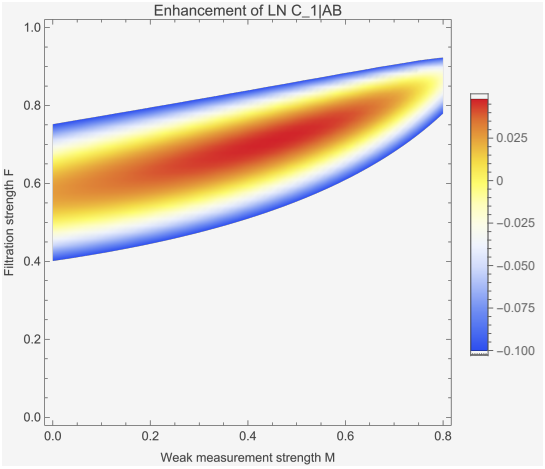
Figure 3: Plot of log negativity of the two bipartitions $A|BC_1$ and $C_1|AB$ obtained by choosing a random value for weak measurement parameter M and filtration parameter F

Figure (3) shows the variation of log negativity of the two bipartitions $A|BC_1$ and $C_1|AB$ with increasing values of T_H at randomly chosen values of the WM parameter M and PNF parameter F. For the plot, the parameters were chosen as $M = 0.2$ and $F = 0.6$. The plot shows that the bipartition $C_1|AB$ experiences a decline in log negativity from 0.860 to 0.538, which is about 37.4% with increasing T_H, while the bipartition $A|BC_1$ experiences a decrease in log negativity from 0.803 to 0.617, which is about a 23% decline in log negativity with increasing value of T_H. By comparing the outcomes in Figure (3) with the outcomes of the case without WM and PNF in Figure (2), it can be seen that there is a slight enhancement in the entanglement in the presence of WM and PNF in comparison with the state without WM and PNF. This brings up the next area of investigation, which is to find out if WM and PNF are always advantageous to entanglement.

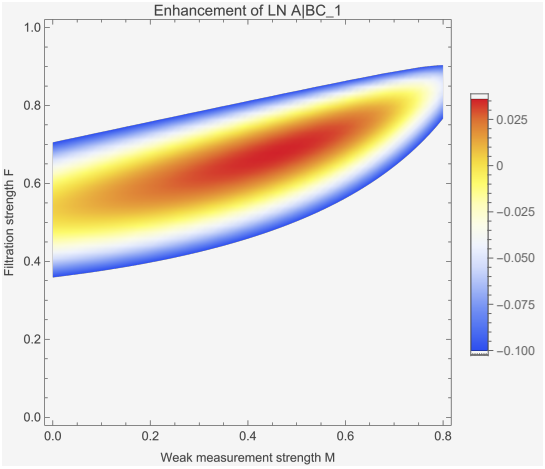
Figure (4) is a density plot of ΔE_N with varying values of M and F; the red part of the plot shows the regions of values of M and F that give the positive values of ΔE_N. From the plot it can be deduced that beneficial ΔE_N can be obtained for any value of M on the condition that the WM is accompanied by PNF with the values of F falling between 0.4 and 0.75. From the plot, it can also be seen that it is possible to have an entanglement advantage with PNF alone even without the WM operation; this can be clearly seen in Figure (4a), which shows that having a filtration advantage in the absence of WM is more likely in the $C_1|AB$ bipartition than in the $A|BC_1$ bipartition. Also, from the plots it can be seen that the higher the value of M, the narrower the range of the values of F that will yield enhancement in entanglement. Also, by looking at the plots in Figure (4), it can be seen that in the case of bipartition $C_1|AB$, the log negativity can be enhanced by up to 0.045, while the $A|BC_1$ can be enhanced by up to 0.035 by varying F and M. This shows that the $C_1|AB$ bipartition has the tendency to benefit more from the WM and PNF operations in the setup under consideration.

Figure (5) shows the characteristics of log negativity while varying M and F. From the plot, it can be seen that to obtain a maximum value of log negativity, F has to increase directly with M; that is, higher values of M must be accompanied by higher values of F.

Figure (6) shows the conditional filtration success probability P_F as M and F vary. Within this conditional definition, changes in the weak-measurement parameter can modify P_F, while stronger post-noise filtration can reduce it. The same P_F applies to both bipartitions because it is a property of the

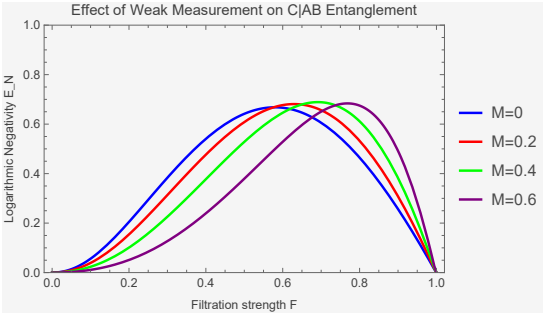


(a) Density plot for bipartition $C_1|AB$

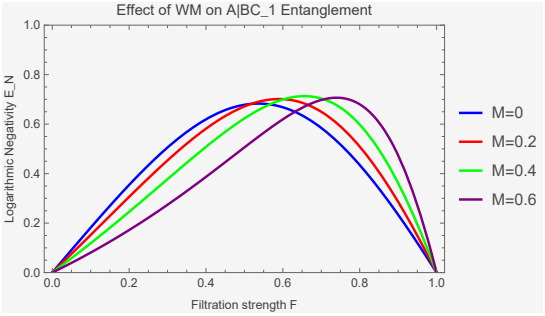


(b) Density plot for bipartition $A|BC_1$

Figure 4: Density plots showing the ranges of weak-measurement parameter M and filtration parameter F and the corresponding changes in logarithmic negativity for the bipartitions $C_1|AB$ and $A|BC_1$



(a) Logarithmic-negativity variations for bipartition $C_1|AB$



(b) Logarithmic-negativity variations for bipartition $A|BC_1$

Figure 5: Plot showing the characteristics of log negativity at different values of M and F for bipartitions $C_1|AB$ and $A|BC_1$

local filtering operation rather than of the bipartition used to evaluate entanglement.

To investigate the values of M and F that give the highest entanglement advantage on the tested numerical grid, a two-dimensional scan was performed over $0 \leq M, F \leq 1$ using increments of 0.1. The logarithmic negativity was evaluated at each grid point while the remaining physical parameters were held fixed.

Table (1) presents the values of fixed parameters used for generating the plots. In Tables (2) and (3), noteworthy values obtained by numerical exploration of the log negativity are presented for each bipartition.

For the reference case $M = 0$ and $F = 0.5$, the logarithmic negativities are 0.630271 for $A|BC_1$ and 0.556614 for $C_1|AB$.

The grid search shows that the parameter choices that maximize logarithmic negativity do not maximize the conditional weighted entanglement yield. For $A|BC_1$, the largest tabulated logarithmic negativity, 0.664254, occurs at $M = 0.5$ and $F = 0.7$, but the corresponding conditional yield decreases from 0.15757 in the reference case to 0.10680. For $C_1|AB$, the maximum tabulated logarithmic negativity, 0.611381, occurs at $M = 0.4$ and $F = 0.7$, with the conditional yield decreasing from 0.139154 to 0.11035. Thus, the preferred values of M and F depend on whether the objective is to maximize conditional entanglement or entanglement yield. Local filtration can nevertheless provide entanglement protection in suitable parameter regimes [45]. Weak-measurement protocols are commonly combined with a subsequent reversal or filtration operation after the noisy channel [46, 47, 48].

At $T_H = 2$, $\gamma = 0.2$, and $p = 0.8$, the $A|BC_1$ bipartition increases from $E_N = 0.630271$ in the reference case to $E_N = 0.664254$ at $M = 0.5$ and $F = 0.7$, corresponding to an enhancement of approximately 5.39%. Its conditional weighted yield decreases by approximately 32.22%. For $C_1|AB$, the logarithmic

Table 1: Model parameters used in the numerical analysis.

Symbol	Physical meaning	Value
θ	Initial-state mixing angle	$\pi/4$
ϕ	Relative phase of the initial state	0
ω	Field-mode frequency	1
γ	Generalised amplitude-damping strength	0.2
p	Environmental excitation probability	0.8
T_H^{fix}	Hawking temperature used for optimisation	2
T_H	Hawking-temperature plotting interval	$0.1 \leq T_H \leq 5$
M	Weak-measurement strength	$0 \leq M \leq 1$
F	Local-filtration parameter	$0 \leq F \leq 1$

The setting $M = 0$ corresponds to no weak measurement, while $F = 0.5$ corresponds to the identity filter and therefore represents the no-filtration condition.

Table 2: Summary of the principal optimisation results of $A|BC_1$ at $T_H = 2$.

Protocol and objective	M^*	F^*	$E_N^{A\|BC_1}$	P_F	$Y^{A\|BC_1}$
No control	0	0.5000	0.630271	0.250000	0.15757
WM alone: best tested nonzero M	0.10000	0.50000	0.631077	0.25000	0.15777
WM and active filtration: maximum on the tested grid	0.5000	0.7000	0.664254	0.160784	0.10680
Filtration alone: tested point $F = 0.6$	0.00000	0.60000	0.620751	0.244544	0.15180

Table 3: Summary of the principal optimisation results of $C_1|AB$ at $T_H = 2$.

Protocol and objective	M^*	F^*	$E_N^{C_1\|AB}$	P_F	$Y^{C_1\|AB}$
No control	0.000000	0.500000	0.556614	0.250000	0.139154
WM alone: best tested nonzero M	0.10000	0.50000	0.54151	0.25000	0.13538
WM and active filtration: maximum on the tested grid	0.4000	0.7000	0.611381	0.180496	0.11035
Filtration alone: tested point $F = 0.6$	0.000000	0.600000	0.592928	0.244544	0.145000

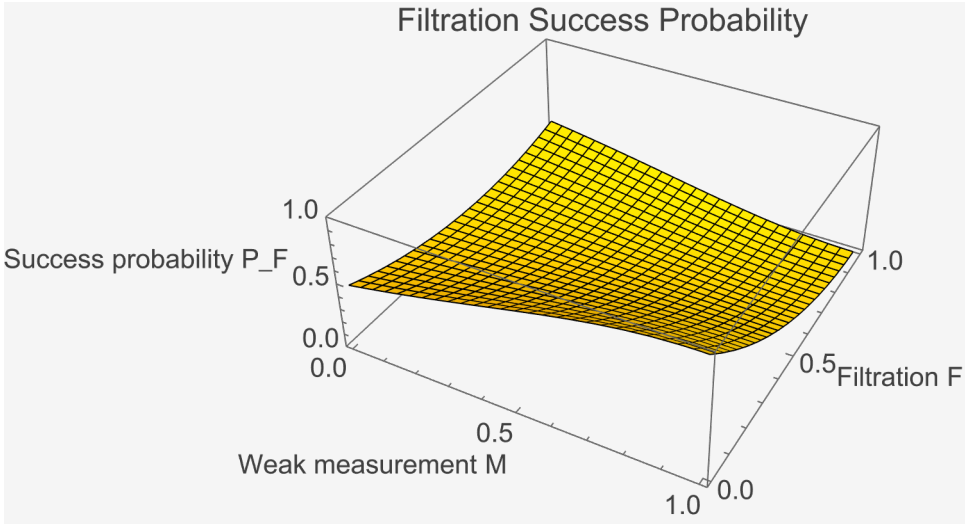


Figure 6: Conditional post-filtration success probability P_F with varying values of M and F

negativity increases from 0.556614 to 0.611381 at $M = 0.4$ and $F = 0.7$, corresponding to an enhancement of approximately 9.84%, while the conditional weighted yield decreases by approximately 20.70%. Under this parameter regime, the relative entanglement enhancement is therefore larger for $C_1|AB$, although it is accompanied by a reduced conditional yield.

5 Conclusion

This work investigates the effect of weak measurement and post-noise filtration on a tripartite entangled Dirac system, with entanglement quantified by logarithmic negativity. Because particles A and B are subjected to identical conditions in the asymptotically flat region, the analysis focuses on the two distinct bipartitions $A|BC_1$ and $C_1|AB$. Particles A and B interact with the GAD channel, while particle C_1 is affected by the Schwarzschild background and Hawking radiation. The results show that suitable combinations of weak measurement and post-noise filtration can increase the conditional logarithmic negativity. The numerical optimization also demonstrates a trade-off: parameter values that maximize conditional entanglement can reduce the conditional filtration success probability and the corresponding weighted entanglement yield. Under the parameter regime considered, the relative increase in logarithmic negativity is larger for $C_1|AB$ than for $A|BC_1$. These results indicate that weak measurement and post-noise filtration can protect entanglement, but their usefulness depends on whether the operational objective prioritizes conditional entanglement or entanglement yield.

Author Contributions

All authors were responsible for the conceptualisation and methodology design; both authors were responsible for writing the code for the research. All authors engaged in the validation, formal analysis, and visualisation of the project, and all authors were involved in the writing, review, and editing of the manuscript.

Conflict of Interest

The authors declare that there is no conflict of interest regarding the publication of this paper.

References

[1] Tianxuan Feng, Zhiying Song, Tong Wu, Xun Lu, and Lijing Li. Quantum entanglement source model pumped by low-power laser diode. In *Conference on Infrared, Millimeter, Ter-*

ahertz Waves and Applications (IMT2022), volume 12565, pages 362–370. SPIE, 2023. doi: https://doi.org/10.1117/12.2662233.

[2] Fei Wang, Chaowen Wang, Kang Shen, and Xiangming Hu. Stable entanglement and one-way steering via engineering of a single-atom reservoir. *Optics Express*, 30(10):15830–15845, 2022. doi: https://doi.org/10.1364/OE.452974.

[3] Divyam Pithawa, Sarthak Nahar, Vivek Bhardwaj, Romil Rawat, Ruchi Dronawat, and Anjali Rawat. Quantum computing technological design along with its dark side. *Quantum Computing in Cybersecurity*, pages 295–312, 2023. doi: https://doi.org/10.1002/9781394167401.ch18.

[4] Xianming Meng. Quantum coherence is the essence of quantum entanglement. *Discover Physics*, 2(1):6, 2026. doi: https://doi.org/10.1007/s44418-026-00007-x.

[5] Haoran Zhang, Haotao Zhu, Ruihua He, Yan Zhang, Chao Ding, Lajos Hanzo, and Weibo Gao. Towards global quantum key distribution. *Nature Reviews Electrical Engineering*, pages 1–13, 2025. doi: https://doi.org/10.1038/s44287-025-00238-7.

[6] Omar Amer, Vaibhav Garg, and Walter O Krawec. An introduction to practical quantum key distribution. *IEEE Aerospace and Electronic Systems Magazine*, 36(3):30–55, 2021. doi: https://doi.org/10.1109/MAES.2020.3015571.

[7] Yuan Cao, Yongli Zhao, Qin Wang, Jie Zhang, Soon Xin Ng, and Lajos Hanzo. The evolution of quantum key distribution networks: On the road to the qinternet. *IEEE Communications Surveys & Tutorials*, 24(2):839–894, 2022. doi: https://doi.org/10.1109/COMST.2022.3144219.

[8] Shalini Subramani, Selvi M, Kannan A, and Santhosh Kumar Svn. Review of security methods based on classical cryptography and quantum cryptography. *Cybernetics and Systems*, 56(3):302–320, 2025. doi: https://doi.org/10.1080/01969722.2023.2166261.

[9] Ishika Giroti and Meenakshi Malhotra. Quantum cryptography: A pathway to secure communication. In *2022 6th International Conference on Computation System and Information Technology for Sustainable Solutions (CSITSS)*, pages 1–6. IEEE, 2022. doi: https://doi.org/10.1109/CSITSS57437.2022.10026388.

[10] Muhammad Imran, Ahmed B Altamimi, Wilayat Khan, Shariq Hussain, Mohammad Alsaffar, et al. Quantum cryptography for future networks security: A systematic review. *IEEE access*, 12:180048–180078, 2024. doi: https://doi.org/10.1109/ACCESS.2024.3504815.

[11] Ahmad Adel Abutaleb. Microscopic unitarity and the quantization of black hole evaporation time. *arXiv preprint arXiv:2601.05305*, 2026. doi: https://doi.org/10.48550/arXiv.2601.05305.

[12] Mahnaz Maleki, Zahra Ebadi, and Hosein Mohammadzadeh. Nonextensive statistics and the entropy on the horizon. *International Journal of Modern Physics A*, 39(04):2450019, 2024. doi: https://doi.org/10.1142/S0217751X24500192.

[13] Thiago T Bergamaschi. A pedagogical approach to the black hole information issue. *Revista Brasileira de Ensino de Física*, 48:e20250192, 2026. doi: https://doi.org/10.1590/1806-9126-RBEF-2025-0192.

[14] Gutivan A Syahputra and Bintoro Anang Subagyo. Thermodynamics of kerr-newman black hole. In *Journal of Physics: Conference Series*, volume 2498, page 012026. IOP Publishing, 2023. doi: https://doi.org/10.1088/1742-6596/2498/1/012026.

[15] Antonio Amariti and Alessia Segati. Kerr-newman black holes from $n = 1*$. *Journal of High Energy Physics*, 2023(6):216, 2023. doi: https://doi.org/10.1007/JHEP06(2023)216.

[16] O Ruiz, U Molina, and P Viloria. Thermodynamic analysis of kerr-newman black holes. In *Journal of Physics: Conference Series*, volume 1219, page 012016. IOP Publishing, 2019. doi: https://doi.org/10.1088/1742-6596/1219/1/012016.

[17] Ran Li. Decoherence of quantum superpositions by reissner-nordström black holes. *Physical Review D*, 111(2):024040, 2025. doi: https://doi.org/10.1103/PhysRevD.111.024040.

[18] Sanjar Shaymatov, Bakhtiyor Narzilloev, Ahmadjon Abdujabbarov, and Cosimo Bambi. Charged particle motion around a magnetized reissner-nordström black hole. *Physical Review D*, 103(12):124066, 2021. doi: https://doi.org/10.1103/PhysRevD.103.124066.

[19] Behnam Pourhassan, İzzet Sakallı, Xiaoping Shi, Mir Faizal, and Salman Sajad Wani. Quantum thermodynamics of an reissner-nordström black hole. *Europhysics Letters*, 144(2):29001, 2023. doi: https://doi.org/10.1209/0295-5075/acfff0.

[20] Ruben Campos Delgado. Quantum gravitational corrections to the entropy of a reissner–nordström black hole. *The European Physical Journal C*, 82(3):272, 2022. doi: https://doi.org/10.1140/epjc/s10052-022-10232-0.

[21] Cookey Iyen, Muhammad Sanusi Liman, Benedict O Ayomanor, Emem-obong Solomon James, Yame Mwanzang Philemon, and Babatunde James Falaye. Quantum fisher information in curved spacetime: Dirac particles in noisy channels around a schwarzschild black hole. *International Journal of Theoretical Physics*, 64(8):205, 2025. doi: https://doi.org/10.1007/s10773-025-06073-8.

[22] Jorge Ovalle, Roberto Casadio, and Alexander Kamenshchik. Schwarzschild black hole singularity formation. *Physical Review D*, 113(6):064042, 2026. doi: https://doi.org/10.1103/cbs6-d7pr.

[23] Roberto Casadio, Alexander Kamenshchik, and Jorge Ovalle. Cosmology from schwarzschild black hole revisited. *Physical Review D*, 110(4):044001, 2024. doi: https://doi.org/ 10.1103/PhysRevD.110.044001.

[24] Yan-Ling Li, Cai-Hong Liao, Lin Yao, and Xing Xiao. Enhancing the teleportation of quantum fisher information under correlated generalized amplitude damping noise. *Results in Physics*, 53:107010, 2023. doi: https://doi.org/10.1016/j.rinp.2023.107010.

[25] Nour Zidan, Atta ur Rahman, and Saeed Haddadi. Quantum teleportation in a two-superconducting qubit system under dephasing noisy channel: role of josephson and mutual coupling energies. *Laser Physics Letters*, 20(2):025204, 2023. doi: https://doi.org/10.1088/1612-202X/acb043.

[26] Yousef Mafi, Ali Kookani, Hossein Aghababa, Masoud Barati, and Mohammadreza Kolahdouz. Bidirectional quantum controlled teleportation in multi-hop networks: a generalized protocol for the arbitrary n-qubit state through the noisy channel. *Quantum Information Processing*, 23(10):350, 2024. doi: https://doi.org/10.1007/s11128-024-04561-0.

[27] Wojciech Górecki, Alberto Riccardi, and Lorenzo Maccone. Quantum metrology of noisy spreading channels. *Physical Review Letters*, 129(24):240503, 2022. doi: https://doi.org/10.1103/PhysRevLett.129.240503.

[28] Jia-Yin Peng, Liang Tang, Zhen Yang, Fan Wu, Zhi-Wen Mo, and Ming-Qiang Bai. Cyclic teleportation in noisy channel with nondemolition parity analysis and weak measurement: J.-y. peng et al. *Quantum Information Processing*, 21(3):114, 2022. doi: https://doi.org/10.1007/s11128-022-03461-5.

[29] Mengting Wang and Hai-Sheng Li. Bidirectional quantum teleportation using a five-qubit cluster state as a quantum channel. *Quantum Information Processing*, 21(2):44, 2022. doi: https://doi.org/10.1007/s11128-021-03389-2.

[30] Sebastian Ecker, Philipp Sohr, Lukas Bulla, Rupert Ursin, and Martin Bohmann. Remotely establishing polarization entanglement over noisy polarization channels. *Physical Review Applied*, 17(3):034009, 2022. doi: https://doi.org/10.1103/PhysRevApplied.17.034009.

[31] Udara Jayasinghe, Namesh Kushantha, Thanuj Fernando, and Anil Fernando. A robust multi-qubit quantum communication system for image transmission over error prone channels. *IEEE Transactions on Consumer Electronics*, 2025. doi: https://doi.org/10.1109/TCE.2025.3594368.

[32] Yuta Kikuchi, Conor Mc Keever, Luuk Coopmans, Michael Lubasch, and Marcello Benedetti. Realization of quantum signal processing on a noisy quantum computer. *npj Quantum Information*, 9(1):93, 2023. doi: https://doi.org/10.1038/s41534-023-00762-0.

[33] Shuo Liu, Ming-Rui Li, Shi-Xin Zhang, and Shao-Kai Jian. Entanglement structure and information protection in noisy hybrid quantum circuits. *Physical Review Letters*, 132(24):240402, 2024. doi: https://doi.org/10.1103/PhysRevLett.132.240402.

[34] Cookey Iyen, Babatunde James Falaye, and Muhammad Sanusi Liman. Scrutinizing joint remote state preparation under decoherence. *Scientific Reports*, 13(1):8066, 2023. doi: https://doi.org/10.1038/s41598-023-34949-4.

[35] C Iyen, MS Liman, SJ Emem-Obong, WA Yahya, CA Onate, and BJ Falaye. Examining the quantum fisher information in the interaction of a dirac system with a squeezed generalized amplitude damping channel. *Scientific Reports*, 14(1):24495, 2024. doi: https://doi.org/10.1038/s41598-024-76007-7.

[36] Chi-Kwong Li, Yuqiao Li, Diane Christine Pelejo, and Sage Stanish. Quantum error correction scheme for fully-correlated noise: C-k. li et al. *Quantum Information Processing*, 22(8):310, 2023. doi: https://doi.org/10.1007/s11128-023-04009-x.

[37] Avimita Chatterjee, Koustubh Phalak, and Swaroop Ghosh. Quantum error correction for dummies. In *2023 IEEE International Conference on Quantum Computing and Engineering (QCE)*, volume 1, pages 70–81. IEEE, 2023. doi: https://doi.org/10.1109/QCE57702.2023.00017.

[38] Weizhou Cai, Xianghao Mu, Weiting Wang, Jie Zhou, Yuwei Ma, Xiaoxuan Pan, Ziyue Hua, Xinyu Liu, Guangming Xue, Haifeng Yu, et al. Protecting entanglement between logical qubits via quantum error correction. *Nature Physics*, 20(6):1022–1026, 2024. doi: https://doi.org/10.1038/s41567-024-02446-8.

[39] Hongzhen Chen, Yu Chen, Jing Liu, Zibo Miao, and Haidong Yuan. Quantum metrology enhanced by leveraging informative noise with error correction. *Physical Review Letters*, 133(19):190801, 2024. doi: https://doi.org/10.1103/PhysRevLett.133.190801.

[40] Mummadi Swathi and Bhawana Rudra. Novel encoding method for quantum error correction. In *2022 IEEE 12th Annual Computing and Communication Workshop and Conference (CCWC)*, pages 1001–1005. IEEE, 2022. doi: https://doi.org/10.1109/CCWC54503.2022.9720880.

[41] Luis Colmenarez, Ze-Min Huang, Sebastian Diehl, and Markus Müller. Accurate optimal quantum error correction thresholds from coherent information. *Physical Review Research*, 6(4):L042014, 2024. doi: https://doi.org/10.1103/PhysRevResearch.6.L042014.

[42] Daiki Komoto and Kenta Kasai. Quantum error correction near the coding theoretical bound. *npj Quantum Information*, 11(1):154, 2025. doi: https://doi.org/10.1038/s41534-025-01090-1.

[43] Swathi Mummadi, Gnaneshwara Chary Udari, C Achyuth, and C Karthik. Error correction methods for protecting quantum information. In *The Quantum AI Era of Neuromarketing*, pages 113–132. IGI Global Scientific Publishing, 2025. doi: https://doi.org/10.4018/979-8-3693-7673-7.ch005.

[44] Wen-Yang Sun, Dong Wang, Bao-Long Fang, Jia-Dong Shi, and Liu Ye. The enhancement of quantum entanglement under an open dirac system with the hawking effect in schwarzschild spacetime. *Laser Physics Letters*, 15(6):065210, 2018. doi: https://doi.org/10.1088/1612-202X/aab69c.

[45] Chunyu Huang, Wenchao Ma, and Liu Ye. Protecting quantum entanglement and correlation by local filtering operations. *Quantum Information Processing*, 15(8):3243–3256, 2016. doi: https://doi.org/10.1007/s11128-016-1328-6.

[46] Meijiao Wang, Haojie Liu, Lianzhen Cao, Yang Yang, Xia Liu, Bing Sun, and Jiaqiang Zhao. Protecting the entanglement of x-type systems via weak measurement and reversal in the generalized amplitude damping channel. *Entropy*, 27(4):350, 2025. doi: https://doi.org/10.3390/e27040350.

[47] Meijiao Wang, Bing Sun, Lianzhen Cao, Yang Yang, Xia Liu, Xinle Wang, and Jiaqiang Zhao. Improving the capacity of quantum dense coding and the fidelity of quantum teleportation by weak measurement and measurement reversal. *Entropy*, 25(5):736, 2023. doi: https://doi.org/10.3390/e25050736.

[48] Xing Xiao, Wen-Rui Huang, Tian-Xiang Lu, and Yan-Ling Li. Protecting three-dimensional entanglement from the correlated amplitude damping channel. *Chinese Journal of Physics*, 97:223–238, 2025. doi: https://doi.org/10.1016/j.cjph.2025.03.027.